TOPICAL REVIEW — Magnetism, magnetic materials, and interdisciplinary research

Energy band alignment at ferroelectric/electrode interface determined by photoelectron spectroscopy*

Chen Feng(陈 峰)[a)†], Wu Wen-Bin(吴文彬)[a)], Li Shun-Yi(李舜怡)[b)], and Andreas Klein[b)]

[a)] High Magnetic Field Laboratory, Chinese Academy of Sciences (CAS), and Hefei National Laboratory for Physical Sciences at Microscale, University of Science and Technology of China, Hefei 230026, China

[b)] TechnischeUniversitt Darmstadt, Department of Materials and Earth Sciences, Petersenstraße 32, D-64287 Darmstadt, Germany

(Received 29 November 2013; published 27 December 2013)

The most important interface-related quantities determined by band alignment are the barrier heights for charge transport, given by the Fermi level position at the interface. Taking $Pb(Zr,Ti)O_3$ (PZT) as a typical ferroelectric material and applying X-ray photoelectron spectroscopy (XPS), we briefly review the interface formation and barrier heights at the interfaces between PZT and electrodes made of various metals or conductive oxides. Polarization dependence of the Schottky barrier height at a ferroelectric/electrode interface is also directly observed using XPS.

Keywords: ferroelectric, band alignment, Schottky barrier, X-ray photoelectron spectroscopy

PACS: 77.55.fg, 73.30.+y, 79.60.Jv, 77.80.Fm **DOI:** 10.1088/1674-1056/23/1/017702

1. Introduction

Energy band alignment at the interfaces of a ferroelectric material is of direct relevance to the material's electrical functions. The most important interface-related quantities that are determined by band alignment are the barrier heights for charge transport, given by the Fermi level position at the interface. X-ray photoelectron spectroscopy (XPS) has played an important role in determining the Fermi level positions at the interfaces of ferroelectrics with different electrodes.

$Pb(Zr,Ti)O_3$ (PZT) is one of the most intensively studied ferroelectric materials due to its small coercive field, large polarization, and high Curie temperature, having applications in piezoelectric sensors, actuators, and non-volatile memories.[1,2] Electrical fatigue — the reduction in polarization with increasing switching cycles — is a critical issue for stable ferroelectric device operation.[3,4] For thin films, both cycling stability and leakage current strongly depend on the electrode material chosen.[5,6] The fatigue of PZT thin film capacitors is particularly pronounced with Pt electrodes, while the use of oxidic electrodes such as $La_{0.5}Sr_{0.5}CoO_3$, $SrRuO_3$, $LaNiO_3$, $La_{0.7}Sr_{0.3}MnO_3$, and RuO_2 leads to less fatigue.[7–11] Different fatigue models and mechanisms have been reviewed by Tangantsev *et al.*[4] and Lou *et al.*[12] Accumulation of oxygen vacancies at the ferroelectric/electrode interface and/or injection of charge carriers through the interface are thought to be related to the fatigue phenomenon. Both effects are directly linked to the PZT/electrode interface properties.

It is known that some interface properties of semiconducting oxides are of practical importance, e.g., for numerous electronic devices like thin film solar cells, (organic) light emitting diodes, thin film transistors, and information technology.[13] The energy band alignment at semiconductor interfaces, probably one of the most important properties of semiconductor heterojunctions, is determined by the Schottky barrier heights at the semiconductor/metal interfaces and by the valence and conduction band discontinuities at the semiconductor heterointerfaces, and it largely defines the potential distribution and the current transport through these interfaces, and thus the functionality of the electronic devices.[14] PZT thin films are usually treated as wide-band semiconductors due to the existence of defects, i.e., oxygen vacancies. For the PZT/electrode interface, the choice of electrode material determines the Fermi level position at the interface, which defines the barriers for the injections of electrons ($\Phi_{B,n} = E_{CB} - E_F$) and holes ($\Phi_{B,p} = E_F - E_{VB}$). Previously, the Fermi level position at the PZT/Pt interface has been derived by Scott *et al.*, using a combination of metal work function and PZT electron affinity, $E_F - E_{VB} = 1.6$ eV.[15] Using the empirical Fermi level pinning mode from Mönch,[16] Robertson and Chen have calculated a value of $E_F - E_{VB} = 1.95$ eV. Note that neither of these values was directly determined experimentally. In addition, they did not take into account possible modifications of the barrier heights by changes in interface chemistry.

In the present work, all the energy band alignments between PZT and different materials are ascertained by *in situ* photoelectron spectroscopy. The experimental procedure will

*Project supported by the German Science Foundation (DFG) within the Collaborative Research Center SFB 595 (Electrical Fatigue of Functional Materials), the National Natural Science Foundation of China (Grant Nos. 11274287, 11174001, and 11204313), and the National Basic Research Program of China (Grant No. 2012CB927402).

†Corresponding author. E-mail: fchen@hmfl.ac.cn

© 2014 Chinese Physical Society and IOP Publishing Ltd

be introduced in the second section.

In the third section (results and discussion), the absolute values for the barrier heights at the PZT/metal interface will be introduced first, and the modification of the barrier height at the PZT/Pt interface upon oxidation and reduction are discussed as well. Further, the interface between PZT and (conductive) oxides will be reviewed. It has been proposed that oxidic electrodes absorb oxygen vacancies,[17,18] leading to less fatigue. However, polarization fatigue has also been observed for n-type conductive electrodes such as In_2O_3:Sn (ITO)[19,20] and $SrSnO_3$:La.[21,22] This strongly suggests that polarization fatigue in the case of PZT is more closely related to the electronic interface properties. This view is also supported by the results of Du and Chen,[23] who observed a greater improvement in fatigue when using a p-type Si barrier, as compared with an n-type Si barrier. Therefore the injection of electrons rather than holes might be related to the PZT fatigue. In bulk form, PZT shows p-type conductivity due to Pb vacancies. Indeed, there has been a dispute in the literature about whether the current transport in PZT thin films is dominated by electrons or holes. However it is commonly believed that the Fermi level position in PZT at the interface corresponds to the zero-field Schottky barrier height for electrons or holes, and due to the low carrier concentration in PZT, it is the contact properties that determine whether the majority electronic carriers in PZT are electrons or holes.[14,16]

In addition, contact between $SrTiO_3$ (STO) and $PbTiO_3$ (PTO) is introduced. STO and PTO are oxide semiconductors with similar band gaps of 3.2 eV[24] and 3.4 eV,[25] respectively. The top of the STO valence band is derived mainly from O 2p states, and the conduction band is largely derived from Ti 3d orbitals. In PTO, the Pb 6s states contribute significantly to both the valence and the conduction bands, which is due to Pb existing in a +2 oxidation state in these compounds.[26,27] Another notable difference between STO and PTO lies in their electrical conductivity behaviors. STO can be made highly n-type, e.g., by reduction or by doping with Nb or La,[28] while bulk PTO is reported to be weakly p-type because of intrinsic doping by vacancies.[29,30] The limits of electric conductivity are mainly attributed to the limits of mobile carrier (electron and hole) concentrations. Since the concentrations of mobile carriers are defined by the energy distance between the Fermi level E_F and the band edges (E_{VB} and E_{CB}),[14] the range of accessible conductivities is directly related to the range of Fermi level positions. This phenomenon is known as self-compensation and is related to the formation of compensating intrinsic defects, like oxygen or cation vacancies and interstitials.[31–34] Attempts have been made to generalize these doping limits for different materials by aligning them on a common energy scale,[32,34] which is best defined by the energy band alignment. From the valence band offset formatted between PTO and STO, in Subsection 4.3 we will see that the estimated energy band alignments obtained from electron affinity measurements, transitivity of barrier heights with various contact materials and the directly determined band alignment are in good agreement with each other. At last, we will introduce an experimental approach based on photoelectron spectroscopy, which allows us to quantitatively determine the Schottky barrier height at a ferroelectric/electrode interface in dependence on polarization.

2. Experimental procedure

A procedure for determining energy band alignment using photoelectron spectroscopy (PES) has been outlined by Waldrop and coworkers,[35] and depicted by Kelin[13] (Fig. 1), and has been extensively used to study semiconductor interface formation.[36,37] Binding energies in PES are measured with respect to the Fermi level of the spectrometer system and can be easily calibrated by measuring the Fermi edge emission of a metallic sample. For semiconductor samples, the onset of emission at a low binding energy corresponds to the valence band maximum (VBM) at a binding energy of $E_F - E_{VB}$. The core levels of the semiconductor should exhibit a binding energy $E_{VB}^{CL} = E_B(CL) - E_{VB}$ with respect to the VBM, which is characteristic (or a constant value) for a given material and can be determined for the substrate and the contact material at the beginning and the end of an interface experiment, respectively. Normally, the interface experiment begins with the preparation of a substrate surface and continues by stepwise deposition of the contact material until the substrate emission lines are completely attenuated. Al $K\alpha$ radiation is used as the excitation source for PES ($h\nu = 1486.6$ eV), which corresponds to a thickness of the contact material of ~ 10 nm. In order to observe the evolution of the chemical and electronic properties, the contact material has to be deposited in multiple steps, starting with films of sub-nanometer thickness.

The procedure of an interface experiment using PES is illustrated in Fig. 1. The valence band discontinuity is derived from the binding energy difference of substrate and film core levels ΔE_{CL}, which can be measured if the thickness of the deposited film is less than 3–5 times the inelastic mean free path of the photoelectrons. The latter is a function of the kinetic energy of the photoelectrons and varies in the range of 0.5–3 nm.[38] In the idealized case, ΔE_{CL} does not depend on the thickness of the deposited film. However, ΔE_{CL} may be nonconstant in the case of strong band bending or if the electronic structure of the deposited film is not yet fully developed, e.g., if the crystallographic structure of the film depends on the film thickness.[39,40] For a reliable determination of band alignment, a series of depositions with stepwise increasing film thickness is therefore recommended. If several core level lines are available, it is also important to check

whether ΔE_{CL} is constant for different substrate and film core levels. Valence band discontinuities can be further determined from photoelectron spectroscopy by valence band difference spectra,[41] although this procedure is less reliable and less frequently applied.

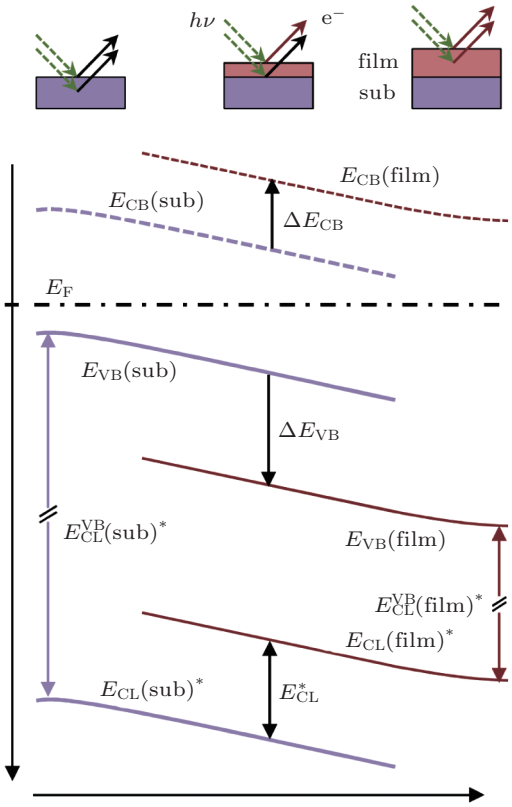


Fig. 1. Determination of energy band alignment between two semiconductors by photo-electron spectroscopy. Experimentally determined quantities are indicated by asterisks.[13]

3. Experiment

The experiments were performed using the integrated surface analysis and preparation system DAISY-MT (Darmstadt Integrated System for Materials Research), which combines a multi-technique surface analysis system (Physical Electronics PHI 5700) and several thin film deposition chambers with an ultrahigh vacuum sample transfer. X-ray photoelectron spectra were recorded using monochromatic Al $K\alpha$ radiation, providing an overall energy resolution of ~ 0.4 eV as determined from the Gaussian broadening of the Fermi edge of a sputter-cleaned Ag sample. Binding energies were given with respect to the same Fermi edge emission with an accuracy of < 100 meV. Charging of the sample during photoemission measurements was not observed. All spectra were recorded using a takeoff angle of 45°. The interface formation was monitored by repeated deposition–analysis cycles.

The PZT thin films of 50 nm thickness were deposited on Si wafers or STO substrates by pulsed laser deposition with an energy density of 1.8 J·cm^{-2} at 10 Hz. The temperature and oxygen pressure were set to 650 °C and 30 Pa, respectively. The PZT target with a nominal composition at Zr/Ti ratio of 52/48 was made by standard solid state reaction. In order to obtain a contamination-free surface prior to the top material deposition, the PZT thin films were heated to 400 °C in 0.5 Pa oxygen for 1 h. Such a cleaning process has also been effectively used for other oxide surfaces.[42] The subsequent depositions of Pt, Cu, Ag, ITO (In_2O_3:Sb), and RuO_2 were all made by magnetron sputtering at room temperature.

4. Results and discussion

4.1. Formation and modification of PZT/Pt interface

Figure 2 shows the XPS survey spectra recorded in the course of stepwise deposition of Pt. The as-prepared film shows emissions from Pb, Zr, Ti, and C. The C emissions are attributed to the typical adsorbed hydrocarbon species, which is corroborated by the binding energy of 285 eV. No significant carbonate emissions are observed. For preparing a clean surface, the PZT sample is heated to 400 °C in 0.5 Pa oxygen for 1 h; after heating no emissions related to carbon are observed, and it remains absent during all Pt deposition steps and subsequent annealing in oxygen atmosphere.

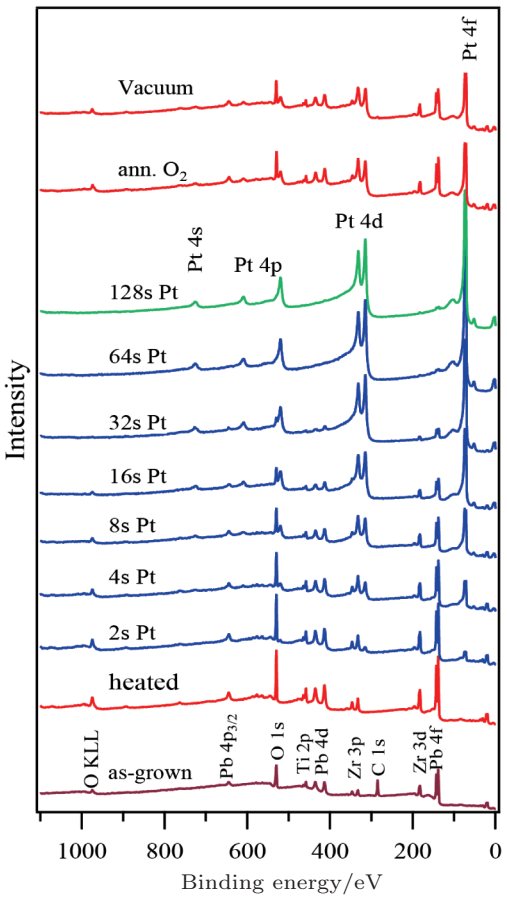


Fig. 2. X-ray photoelectron survey spectra recorded during stepwise deposition of Pt onto Pb(Zr,Ti)O_3. The deposition times are indicated. The growth rate of Pt is ~ 5 nm/min.[70]

The substrate emission intensity decreases and the Pt emission intensity increases during stepwise deposition of Pt. This is also observed in the core level spectra, as shown in Fig. 3. After 128 s deposition of Pt ($\sim$ 10 nm), all substrate emissions are completely attenuated and the spectra show only emissions related to Pt. The deposition of Pt leads to a partial decomposition of the PZT substrate as evident from the Pb 4f spectra, which exhibits a single doublet structure with a binding energy of the $4f_{7/2}$ component of 138.4 eV. This energy corresponds to the oxidized Pb species and is thus attributed to the clean PZT substrate. Note, however, that the absolute binding energy of the PZT film depends on the chosen substrate due to the different energy level alignments at the substrate/PZT interfaces.

The shapes of the Zr 3d, Ti 2p, and O 1s core levels do not change during deposition. However, after the deposition of Pt for 4 s, a second Pb component at lower binding energy already appears, and it becomes more intense with respect to the oxidic Pb component with increasing deposition time. The binding energy of the second species is 136.9 eV, which is typical for a metallic lead.[43,44] With increasing deposition time, the metallic Pb species is also attenuated. This indicates that the metallic Pb remains at the interface and is not floating on the surface of the growing Pt film. The metallic Pb might, however, be partially dissolved in the Pt film due to the slightly negative heat of solution.

The PZT emissions reappear and the Pt 4f intensity decreases after the post-annealing that follows the final Pt deposition step. This is attributed to the island formation in the Pt film and is a typical phenomenon for oxide/Pt interfaces.[42,45] The changes induced in the Pb 4f and Ti 2p core levels by the post-deposition treatments are illustrated in Fig. 4. A lowering of the intensity of the metallic Pb component and a decrement in the binding energy of the oxide Pb species are observed after annealing in oxygen at 400 °C. No changes in the line shape of Ti 2p (and other PZT substrate core levels) are observed. The binding energies of Ti 2p and other core levels are reduced after the oxygen annealing. The Pt 4f emission does not change its shape and binding energy after oxygen annealing. The formation of Pt oxides is therefore excluded. Moreover, after storing the sample for 2 weeks in vacuum (10^{-6} Pa) at room temperature, the energy difference between the oxidic and the metallic Pb components increased considerably. The binding energy of the Ti 2p (and other PZT core levels) emission increased by $>$ 1 eV. After heating the sample in vacuum (10^{-5} Pa) at 400 °C for 30 min, the binding energy of the oxidic Pb 4f peak and Ti 2p peak decreased again.

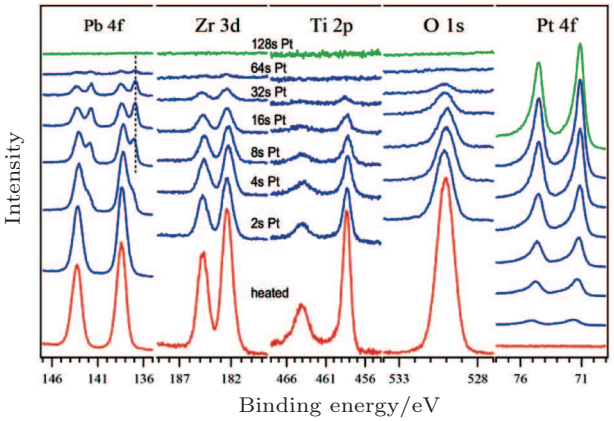


Fig. 3. X-ray photoelectron core level spectra of PZT in the course of Pt deposition. The dashed line in the left graph indicates the binding energy of metallic Pb.[70]

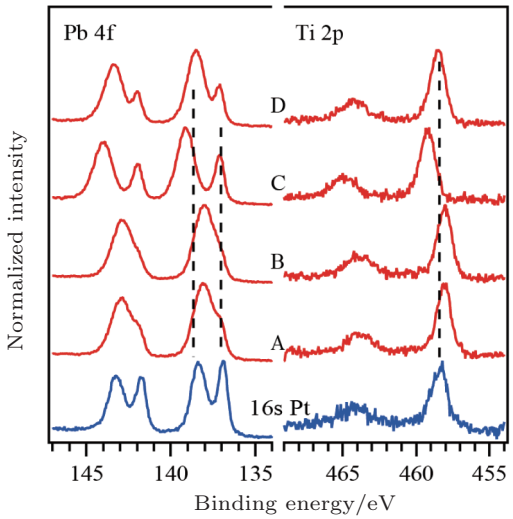


Fig. 4. Pb 4f, Ti 2p, and Zr 3d core level spectra of PZT after deposition of $\sim$ 1 nm Pt (bottom spectra). Other spectra are recorded after $\sim$ 10 nm Pt deposition and different post-deposition treatments: (A) heating in 0.1 Pa oxygen at 400 °C for 30 min, (B) heating in 1 Pa oxygen at 400 °C for 30 min, (C) storage in vacuum ($< 10^{-6}$ Pa) at room temperature for 2 weeks, (D) heating in vacuum (10^{-5} Pa) at 400 °C for 30 min. The spectra are normalized for better comparison. Dashed lines are drawn to emphasize the binding energy shifts.[70]

The PZT-related core level emissions, including the oxidic Pb 4f component, exhibit parallel binding shifts during all deposition steps and post-deposition treatments as shown in Fig. 5. The binding energy shifts of these emissions are therefore attributed to changes in the Fermi level position with respect to the band edges of PZT and hence to changes in the barrier height at the PZT/Pt interface. For the determination of the absolute value of the Fermi level position at the interface, the binding energy difference of the PZT core levels with respect to the PZT VBM of the uncovered PZT substrate is required.[35] The valence band spectrum of the clean, uncovered PZT substrate with the determination of the VBM position is shown in the inset of Fig. 5. The binding energy of the valence band maximum is derived as $E_F - E_{VB}$ = 1.6±0.1 eV. An identical value is reported by Scott *et al.*,[15] although the agreement is considered merely coincidental due to the dependence of binding energies on the substrate. The core level to

VBM binding energies are derived with the VBM energies as 136.7 eV for Pb $4f_{7/2}$, 180.7 eV for Zr $3d_{5/2}$, 456.6 eV for Ti $2p_{3/2,}$ and 528.3 eV for O 1s. The difference between the binding energies are comparable to those reported by Takatani *et al.*,[46,47] which were also determined from a thin PZT film grown on a Pt substrate.

The Fermi level positions of the differently treated interfaces can then be extracted from Fig. 5: $E_F - E_{VB} = 1.6 \pm 0.1$ eV for the interface obtained directly after Pt deposition, 1.25 ± 0.1 eV for the interface annealed in 0.1 Pa oxygen at 400 °C for 30 min, 1.1 ± 0.1 eV for the interface annealed in 1 Pa oxygen at 400 °C for 30 min, 2.2 ± 0.1 eV for the interface stored in vacuum at room temperature for 2 weeks, and 1.55 ± 0.1 eV for the interface heated in vacuum (10^{-5} Pa) at 400 °C for 30 min. These values correspond to the Schottky barrier heights for holes $\Phi_{B,p}$. The barrier heights for electrons are obtained by subtracting these values from the PZT energy gap of $E_g = 3.4$ eV.[25]

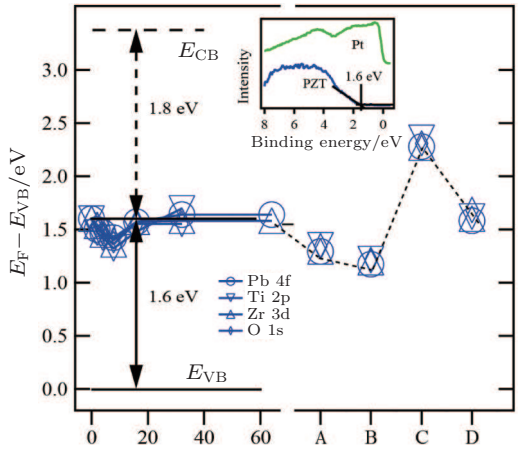


Fig. 5. Binding energies of PZT-related Pb 4f, Ti 2p, Zr 3d, and O 1s core levels in the course of Pt deposition and post-deposition treatments: (A) heating in 0.1 Pa oxygen at 400 °C for 30 min, (B) heating in 1 Pa oxygen at 400 °C for 30 min, (C) storage in vacuum ($< 10^{-6}$ Pa) at room temperature for 2 weeks, (D) heating in vacuum (10^{-5} Pa) at 400 °C for 30 min. The inset shows the valence band spectra recorded from the clean PZT substrate and a thick Pt layer. Core level to valence band maximum binding energy differences are subtracted to reveal directly the Fermi level position at the PZT/Pt interface.[70]

Due to the island formation in the Pt film after the first heating, the surface potential measurements and hence the determination of the barrier heights might be affected by lateral potential inhomogeneities.[42,48–50] However, due to the low doping of the PZT film, the lateral extension of the space charge layer is expected to be large compared with the distance between the Pt islands. Under such a condition, the bands are basically flat along the surface and the measured binding energies of the PZT emissions, which originate mainly from the regions between the Pt islands, are expected to represent the Fermi level position under the Pt islands at the PZT/Pt interface and hence the Schottky barrier height.

The variation of the Schottky barrier height is obviously related to the changes in the chemical composition of the interface. The changes in the chemical composition and electronic structure at the PZT/Pt interface upon annealing in different atmospheres have already been shown by Takatani *et al.*[46,47] Oxidation and reduction of the interface, as apparent from the intensity changes in the metallic Pb species, lead to a reversible decrease and increase in the barrier height for holes. The reduction of the PZT substrate during the initial Pt deposition is attributed to the heat of condensation of the Pt atoms on the surfaces, although the dissolution of Pb in Pt might contribute to the chemical decomposition of the substrate.[51] Comparable effects have been observed during Pt deposition on a variety of substrates.[42,45,52,53] The kinetic energy of the deposited Pt atoms resulting from sputter-deposition may also contribute to the decomposition of the PZT.[54] However, as the evaporation of Pt also leads to the decomposition of the substrate, this is not assumed to be crucial.

After Pt deposition, the interface can be reversibly oxidized and reduced by treatments in different atmospheres. The oxidation and reduction are accompanied by a decrease and increase in the Fermi level position at the interface, as also observed for other oxide/metal combinations.[42,45,55] The variation of the Fermi energy at the interface is believed to be related to changes in interfacial defect concentration caused by the presence of oxygen vacancies, and this seems to be universal, or nearly so, for oxide/metal interfaces.

The strong reduction of the interface after storage at room temperature is, however, a quite notable effect which might have important consequences for the stability of such structures. This might be induced by a decrease in the hydrogen concentration in the Pt film, and three-phase boundaries between PZT, Pt, and the gas phase might also play a role in the chemical changes of the interface.

4.2. Fermi level pinning at PZT/metal interface

Copper and silver were stepwise deposited on PZT thin film surfaces, just as we did with Pt. Details of this part also can be found in Ref. [56]. Figure 6 shows the X-ray induced Pb 4f and O 1s photoelectron core level spectra of the PZT substrate and Pt 4f, Cu $2p_{3/2}$, and Ag $3d_{5/2}$ core levels of the deposited metals recorded in the courses of Pt, Cu, and Ag deposition. The binding energies of the Zr 3d and Ti 2p core levels shift in parallel with the oxide Pb 4f component. The Pb 4f emissions of the clean PZT substrates exhibit a single doublet structure, related to oxidized Pb in PZT (Pb^{2+}). Slightly different binding energies of the PZT substrate emissions may be attributed to weak sample charging or to slightly different conditions of the substrate/PZT interface. Different charging of the samples may result from different thicknesses of the nominally insulating films or from varying substrate condi-

tions during the growth of the PZT films. The constant line shapes and widths of core levels from PZT, which are the Zr 3d, Ti 2p, and the Pb^{2+} 4f emissions, indicate that the formed barriers have a unique value and do not change along the surface.

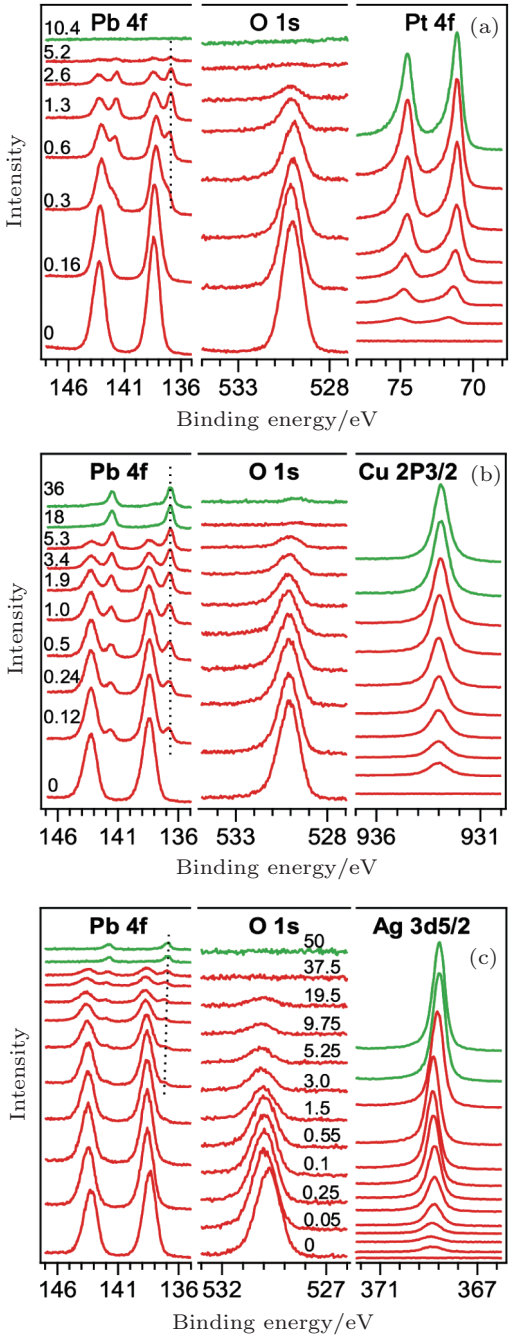


Fig. 6. X-ray photoelectron core level spectra of PZT thin films in the courses of depositing (a) Pt, (b) Cu, and (c) Ag. The core level spectra of Ti 2p and Zr 3d are omitted. The dashed lines indicate metallic Pb. The thicknesses of different metallic films are given in units of nanometer.[56]

The deposition of all three metals leads to a partial decomposition of the PZT substrate, as evident from the observation of a metallic Pb component, which is indicated in Figs. 6(a)–6(c) by dashed vertical lines. The metallic Pb component appears at a binding energy of $\sim$ 137 eV and is most pronounced for the Cu deposition. The weakest intensity of metallic Pb is observed for the Ag deposition. An interface reaction is not expected in view of bulk thermodynamics, as the metal oxides of Pt, Cu, and Ag have only low heats of formation. Copper has the largest heat of formation of metal oxide among the studied contact metals. This corresponds to the largest amount of metallic Pb observed during the deposition of Cu, suggesting that the metal oxide formation contributes to the decomposition of the substrate. No formation of the oxides of Pt, Cu, or Ag is observed, however, in the XP spectra.

In interface experiments using XPS, a decomposition of the substrate has been observed even if the contact partners do not react in the bulk,[51] which has been related to the condensation energy of the deposited species.[57] This has to be expected, particularly for the deposition of atomic species, as is the case for magnetron sputtering or thermal evaporation of metals. Rao *et al.* have explicitly calculated the binding energy of Pt on $BaTiO_3$ to be 4 eV,[58] which exceeds the vacancy formation energy in the bulk.[59] As the vacancy formation at surfaces is typically less expensive than that in the bulk due to the lower coordination number, the reduction of the substrate at the surface becomes even more favorable.

Additional energy gain favoring the substrate decomposition may come from the dissolution of substrate metal atoms in the growing metal film. Enthalpies of solutions of Pb in Pt, Cu, and Ag have been calculated as -16 kJ·mol^{-1}, $+23$ kJ·mol^{-1}, and $+9$ kJ·mol^{-1}, respectively.[60] Intermetallic Pt–Pb phases such as $Pt_{5-7}Pb$[61] and $Pt_{3-4}Pb$[62] are also believed to serve as nucleation seeds for PZT (111) orientation during the growth of PZT on Pt. As an additional term, the surface energy of the deposited materials might be lowered by the segregation of the substrate species to its surface (surfactant effect).

The evolution of the intensity of the metallic Pb species is not the same for the three metals, as is also evident from Fig. 6. While the metallic Pb is attenuated with increasing Pt deposition, its intensity saturates in the cases of Cu and Ag deposition. The behavior of Cu and Ag is explained by Pb floating on the top of the growing film, and the metallic Pb remains at the interface or is dissolved in the growing Pt film. The differing behaviors of the metallic Pb species are in accordance with the different enthalpies of solutions of Pb in Pt, Cu, and Ag. Lead is expected to dissolve only in Pt while the positive heat of solution with Cu or Ag results in a segregation of Pb. The binding energies of Pt $4f_{7/2}$, Cu $2p_{3/2}$, and Ag $3d_{5/2}$ lines for the thick Pt, Cu, and Ag films are 71.1 eV, 932.7 eV, and 368.3 eV, respectively, which are the same as the binding energies of the clean metals.[44] The O 1s core levels are attenuated after the final Pt and Ag deposition but not for the Cu covered sample, where a small signal around 529.7 eV remains. Such a behavior has also been observed during Cu

and Au deposition onto (Ba,Sr)TiO_3.[59] The O 1s signal does not decrease after the final Cu deposition, suggesting that the remaining O 1s comes from oxygen on the surface of the Cu film. Such surface oxygen is noticed only for the case of Cu deposition, which also leads to the largest amount of metallic Pb. The source of oxygen is therefore attributed to the chemical reduction of the PZT substrate.

The Fermi level positions at the interfaces are required to determine the Schottky barrier height. They are derived from the core level binding energies by subtracting the binding energy differences of the PZT core levels with respect to the PZT VBM of the uncovered substrates, as shown in the experimental procedure section. The difference between the binding energy of the core level and the VBM is constant for a material, and it should not change during metal deposition unless a strong chemical disruption of the substrate occurs.[35,63,64] Figures 7(a)–7(c) present the parallel shifts during metal deposition for all three interfaces. Due to the parallel shift of these binding energies, it is safe to attribute them to emissions from a structurally intact PZT substrate and hence to shifts of the Fermi level position with respect the PZT VBM. The starting positions of the VBM of the cleaned PZT films are derived from the XPS spectra before metal deposition, which are shown in the insets of Fig. 7. Any charging effect during the photoemission of the uncovered PZT films will not affect the barrier height determination, as the deposited metal layer will create a short circuit between the surface and the sample holder. The latter defines the binding energy reference. The Fermi level equilibration (electrical contact) of the surface and the sample holder is justified by the fact that the binding energies of the core levels of the deposited metals correspond to their reference values. Therefore, the Fermi level is at zero binding energy after metal deposition. The binding energy of the VBM after metal deposition is extracted from the binding energy before deposition plus the change in binding energy of the core levels during deposition, corresponding to $E_F - E_{VB}$ at the interface, which is the Schottky barrier height for holes.

As is also observed for the Pb 4f emission, the VBM binding energies of the three PZT thin films before metal deposition are slightly different, which may be attributed to different sample charging or to slightly different conditions of the substrate/PZT interface. The Fermi level position at the interface with the deposited metal is derived from the plots in Fig. 7 for a metal thickness with which the shifts of the core level binding energies saturate. The Fermi levels are $E_F - E_{VB} = 1.6 \pm 0.1$ eV, 1.8 ± 0.1 eV, and 1.7 ± 0.1 eV at the PZT/Pt, PZT/Cu, and PZT/Ag interfaces, respectively. These values directly correspond to the Schottky barrier heights for holes, while the Schottky barrier heights for electrons are calculated using a band gap of 3.4 eV as $E_{CB} - E_F = 1.8 \pm 0.1$ eV, 1.6 ± 0.1 eV, and 1.7 ± 0.1 eV, respectively. Considering the experimental uncertainty, the Fermi levels at the interfaces are more or less at the same position for all three metals. This result is in very good agreement with the similarity of leakage currents for these materials.

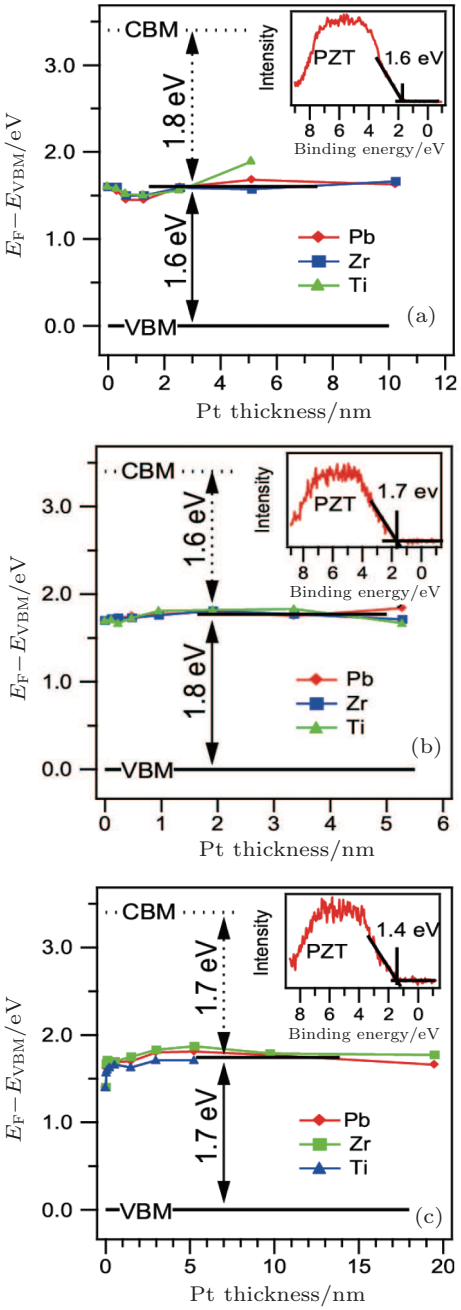


Fig. 7. Evolution of the PZT core level lines with increasing (a) Pt, (b) Cu, and (c) Ag thicknesses. The distance between core levels and the VBM has been subtracted. The VBM and CBM refer to the band edges of PZT. The insets indicate the X-ray photoelectron valence band spectra of the uncovered PZT films used for each interface formation experiment. The Schottky barrier height for holes, $\Phi_{B,p,}$ corresponds to the distance between Fermi level E_F and the VBM E_{VBM}.[56]

The energy band diagrams of the three different PZT/metal interfaces are summarized in Fig. 8. The vacuum level, which is included in Fig. 8, is derived from the work functions of 5.65 eV, 4.65 eV, and 4.25 eV for Pt, Cu, and Ag,

respectively, and an ionization potential of PZT of 6.8 eV. The possible band bending in the PZT substrate is not included in the graphs, as the absolute Fermi level position in the interior of the film is uncertain, due to possible charging effects. Due to the low doping of the PZT film, it is also reasonable to assume that the films are fully depleted. The energetic situation at the investigated PZT/metal interfaces is, however, not affected by this uncertainty as the Fermi level of the deposited metal serves as the binding energy reference. The barrier heights at the interfaces are derived from the XPS measurements described above. The differences in contact potential for the three different metals are mainly compensated by large interface dipole potential drops. They are 0.45 ± 0.1 eV for PZT/Pt, -0.35 ± 0.1 eV for PZT/Cu, and -0.84 ± 0.1 eV for PZT/Ag.

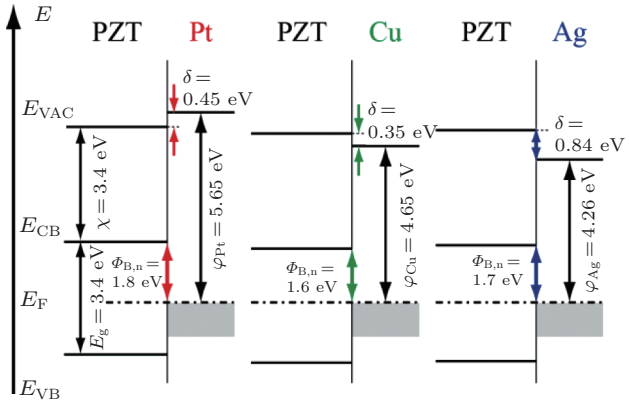


Fig. 8. Band diagram of PZT/Pt, PZT/Cu, and PZT/Ag interfaces containing interface states reflected by the dipole potential δ. The electron affinity $\chi = 3.4$ eV of the cleaned PZT thin films is derived from the UPS measurement and an energy gap of 3.4 eV. By considering the Schottky barrier heights for electrons at the interfaces and taking work functions of 5.65 eV, 4.65 eV, and 4.26 eV for Pt, Cu, and Ag, respectively, into account, the dipole potential δ can be derived from the discontinuity of the vacuum level E_{VAC} at the interface. Here E_{CB}, E_F, and E_{VB} refer to the conduction band, Fermi level, and valence band of PZT, respectively.[56]

Fermi level pinning is a well-known phenomenon for semiconductor interfaces, and it is particularly pronounced for covalently bonded semiconductors such as Si and III–V compounds.[65] The Fermi level pinning is related to the induced gap states, which occur at semiconductor interfaces due to the wave function matching, leading to an exponentially decaying wave function in the semiconductor energy gap.[66] For a high density of induced gap states, the Fermi level at the interface is pinned close to the charge neutrality level of the induced gap states,[67] which has been derived by evaluating branch point energies or dielectric midgap energies.[68,69] Charge neutrality levels for high permittivity oxides have been calculated by Robertson and Chen.[70] The levels for $PbTiO_3$ and $PbZrO_3$ are given as $E_{CNL} - E_{VB} = 1.9$ eV and 2.6 eV, respectively. The former corresponds well with the Schottky barrier height determined for PZT in this work. The samples used in the experiments, however, have a Zr/Ti ratio of nearly 1. If the charge neutrality level scales linearly with the composition, an $E_{CNL} - E_{VB} \approx 2.35$ eV is estimated based on the values of Robertson and Chen. This is significantly higher than the observed Fermi level position at the three interfaces.

Extrinsic defects can considerably affect the barrier heights.[42,45,71,72] It is therefore only reasonable to compare charge neutrality levels with experimental Schottky barrier heights for interfaces with low concentrations of extrinsic defects. As the defects are related to the chemical reduction of the interface, it is likely that these are related to oxygen deficiency. Hence, the lowest defect concentrations are expected for most oxidizing conditions, which consistently leads to a downward shift of the Fermi energy at the interface,[42,45,71] corresponding to a lowering of the hole Schottky barrier. The lowest Fermi level position observed at the PZT/Pt interface is $E_F - E_{VB} = 1.1$ eV,[71] which is significantly lower than the charge neutrality level calculated by Robertson and Chen.[70] Due to the large deviation between the charge neutrality level and the Schottky barrier height for nearly defect-free interfaces, it is suggested that Fermi level pinning by the induced gap states is not pronounced for the PZT/metal interfaces. This is in agreement with the large variation of Schottky barrier heights of PZT with RuO_2 and Sn-doped In_2O_3 (see next subsection), where oxygen deficiency is not expected to play a role. The observed Fermi level pinning at the PZT/metal interface is consequently ascribed to extrinsic defects at the interface. Due to the observed chemical reduction of the PZT, oxygen vacancies are the most likely candidates for these defects.

4.3. Interface between PZT and conductive oxide electrodes

Conductive oxides RuO_2 and ITO are stepwise deposited onto cleaned PZT substrates and the binding energies of the core levels are measured after each step with XPS without breaking the vacuum. The Schottky barrier is also determined by the position of the Fermi level in PZT at the interface. As shown in the inset of Fig. 9, the VBM of the PZT sample lies at 1.7 ± 0.1 eV. In Fig. 9, the evolution of the PZT substrate core level lines during the stepwise deposition of RuO_2 is shown. The difference between core level binding energies and the VBM obtained from the uncoated substrate is subtracted. The shifts of the core level binding energies saturate at $E_F - E_{VB} = 1.0 \pm 0.1$ eV for RuO_2 of thickness > 1 nm. The Schottky barrier height for holes $\Phi_{B,p}$ and electrons $\Phi_{B,n}$ can therefore directly be extracted, amounting to 1.0 ± 0.1 eV and 2.4 ± 0.1 eV for the PZT/RuO_2 interface.

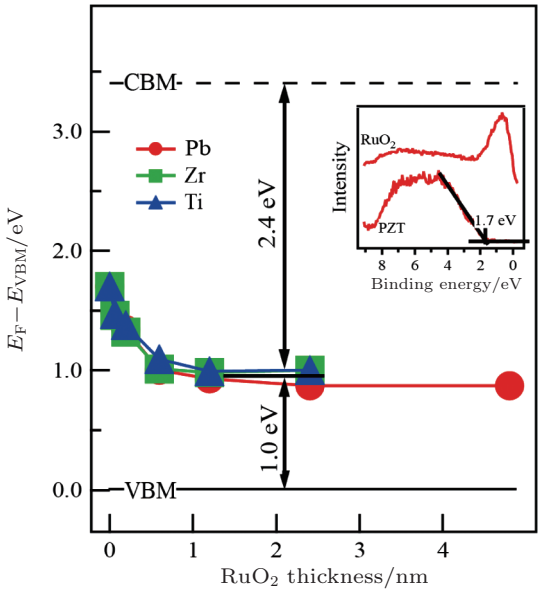


Fig. 9. Evolution of the PZT core level lines with increasing RuO_2 thickness. The distance between the core level lines and the VBM has been subtracted. The inset shows the X-ray photoelectron valence band spectra of the uncovered PZT film and the 10 nm thick RuO_2 film grown on the PZT substrate.[73]

The band alignment between PZT and ITO is determined from the evolution of the PZT and ITO cation emissions with increasing ITO thickness, as presented in Fig. 10. In the inset, the valence band spectra of the uncovered PZT film and the 12 nm thick ITO film grown on PZT are shown. The VBM positions are derived from the leading edges of the valence bands and lie at 2.3 ± 0.1 eV and 3.25 ± 0.1 eV for the uncoated PZT and thick ITO, respectively. In the ITO valence band spectrum, the emission at the low binding energy side of the VBM at $\sim$ 2–3 eV binding energy can be explained by partially unsaturated cations.[43] The PZT sample with 200 nm thick is used in determining the Fermi level at the PZT/ITO interface, which shows a 0.6 eV higher VBM position than that of the 50 nm thick PZT used in the PZT/RuO_2 interface, indicating a slight charging of the thicker PZT film. Due to the parallel shift of substrate and overlayer binding energies, as discussed with regard to the PZT/metal interface, the band alignment can be reliably determined. The discontinuity of binding energy evolution between 0.5 nm and 1 nm thick ITOs is explained by the compensation of the charging effect: once the thickness of the ITO exceeds a certain limit, it becomes conductive enough to short circuit the sample surface with the electrically grounded sample holder. The compensation of the charging effect is verified by the VBM binding energy of the thick ITO film, which is within the range expected for comparable prepared films. This guarantees that the barrier height for charge injection, which is given by the Fermi level position at the interface, is not affected by charging and can thus be directly derived from Fig. 10, where the Fermi level position at the PZT/ITO interface $E_F - E_{VB} = 2.1 \pm 0.2$ eV is deduced for the ITO with thickness > 1 nm. The Fermi level at the PZT/ITO interface is thus in the upper half of the band gap. Since the PZT core level lines do not completely saturate at larger ITO thicknesses, a higher margin of error is assumed. By taking the band gap of PZT of 3.4 eV into account, a Schottky barrier for electrons of 1.3 ± 0.2 eV is derived. Furthermore, a valence band offset between PZT and ITO of 1.1 ± 0.1 eV is derived with the ITO VBM lying at lower binding energies.

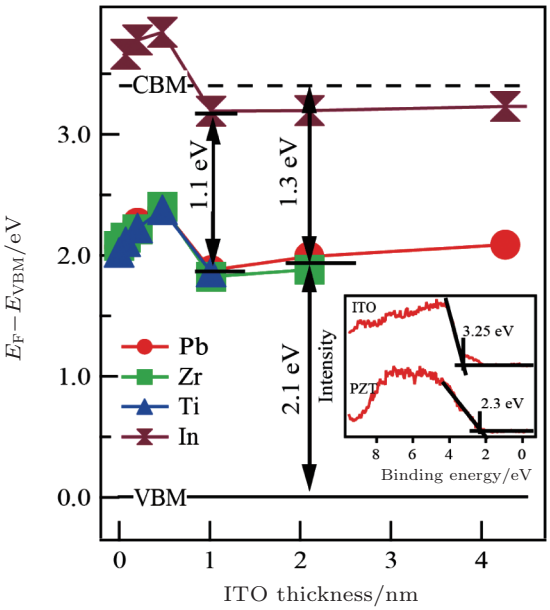


Fig. 10. Evolution of the PZT core level lines with increasing ITO thickness. The distance between the core level lines and the VBM has been subtracted. The inset shows the X-ray photoelectron valence band spectra of the uncovered PZT film and the 12 nm thick RuO_2 film grown on the PZT substrate.[73]

The 1.1 eV difference of the Fermi level positions at the contacts between PZT and RuO_2 and between PZT and ITO is almost as large as the difference in the work functions of RuO_2 and ITO of 1.6 eV. This points to a less strong Fermi level pinning for PZT with oxide electrodes than that calculated by Robertson and Chen using charge neutrality levels (CNLs).[70] They derived a pinning index of 0.31 for $PbTiO_3$ and 0.4 for $PbZrO_3$, which gives $\sim$ 0.4–0.64 eV difference in barrier height for RuO_2 and ITO. This is considerably less than the experimentally found value of 1.1 eV. It is also astonishing that the Fermi level at the contact between RuO_2 and PZT is just 1 eV above the VBM. In the case of the (Ba,Sr)TiO_3/RuO_2 interface, the Fermi level lies $\sim$ 2.3 eV above the VBM.[74] The CNLs for $SrTiO_3$ and $PbZrO_3$ calculated by Robertson are both at 2.6 eV above the VBM, while the CNL for $PbTiO_3$ is calculated to lie at 1.9 eV.[26] For an almost equal mixture of $PbTiO_3$ and $PbZrO_3$, as used for this study, a higher Fermi level position would be expected at the PZT/RuO_2 interface in theory.

A schematic energy band diagram of the deposited PZT/ITO, together with the PZT/RuO_2 contact, is given in Fig. 11. In the case of the PZT/RuO_2 interface, a Schottky

barrier for holes of 1.1 ± 0.1 eV is found. For the PZT/ITO interface, a Schottky barrier for electrons of 1.3 ± 0.2 eV is derived. This shows that using different oxide electrode materials allows for engineering the contact properties. For the PZT, a transition from a preference for hole injection to a preference for electron injection can be achieved when switching from RuO_2 electrodes to ITO electrodes.

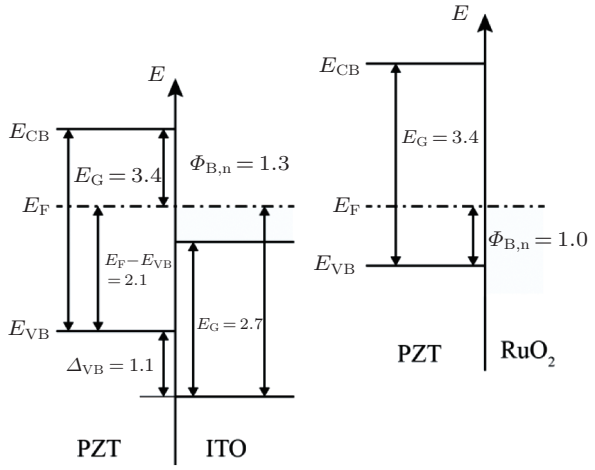


Fig. 11. Schematic band diagram of the PZT/ITO contact (left) and the PZT/RuO2 contact (right). The ITO is a degeneratively doped semiconductor having a fundamental band gap of ∼ 2.7 eV with the Fermi level lying in the conduction band, as also confirmed by the VBM position of 3.25 eV. All the energies are given in units of eV.[73]

4.4. $PbTiO_3$/$SrTiO_3$ interface

Due to the perfect lattice match between $SrTiO_3$ (STO) and $PbTiO_3$ (PTO), PTO films grown on STO substrates are intensively studied. The valence band offset ΔE_{VB} between STO and PTO is first derived based on the transitivity rule. Transitivity is given when the band offsets between materials *A* and *B* and between materials *B* and *C* add up to the band offset between materials *A* and *C*.[75] The difference of the Fermi energy position at the interface of STO and PTO with various materials provides an estimate for the PTO/STO band alignment. The validity of transitivity in the case of the STO/PTO contact will be verified by the direct band alignment shown in this section. Details about the PTO/STO interface can be found elsewhere.[76]

Barrier heights between $SrTiO_3$, $Pb(Zr,Ti)O_3$, or $(Ba,Sr)TiO_3$ and different contact materials are determined with *in situ* photoelectron spectroscopy. Pt, RuO_2, and Sn-doped In_2O_3 are deposited stepwise onto the substrate by using magnetron sputtering. The substitution with isovalent atoms Zr and Ba does not lead to any observable shift of the band edge energies, since the band gaps of both materials are almost unaffected. It is therefore expected that the barrier heights determined for BST or PZT should be essentially identical to those of STO or PTO.

In general, the barrier heights of $SrTiO_3$ (or $(Ba,Sr)TiO_3$) and $Pb(Zr,Ti)O_3$ with the three contact materials all show a difference larger than 1 eV, as shown in Fig. 12. For the BST/Pt and the PZT/Pt interfaces, the Fermi level position depends on the oxidation state. When Pt is deposited, reduction takes place at the surface, leading to the formation of oxygen vacancies and therefore the Fermi levels closer to the conduction band (dash-dotted line). By annealing the sample in oxygen, the interface is oxidized and the defect concentration can then be reduced, leading to a downward shift of the Fermi level closer to the valence band. For a reduced interface, the barrier height difference is slightly larger than that of an oxidized interface.

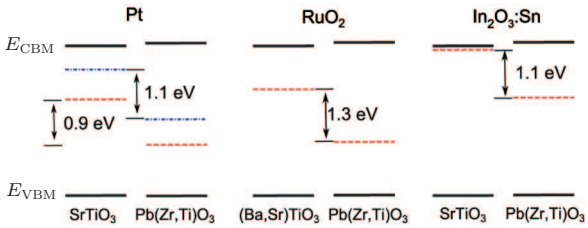


Fig. 12. Fermi level positions at interfaces of $(Ba,Sr)TiO_3$ and $Pb(Zr,Ti)O_3$ with the electrode materials Pt, RuO_2, and In_2O_3:Sn. Depending on processing, reduced (dash-dotted line) and oxidized (dash line) states of the Pt interface can exist, having high and low Fermi level positions, respectively. The distance between the interface Fermi level positions in STO and PTO is shown for the different electrode materials. Here E_{CB} and E_{VB} are conduction band minimum and valence band maximum positions, respectively.[76]

The similarity of the barrier height differences among all three different contact materials indicates that the Fermi level positions at BST and PZT interfaces are certainly transitive. The valence band maximum of PTO (or PZT) is thus approximately 1.1 eV higher in energy than the valence band maximum of STO (or BST).

In order to verify the transitivity shown by the barrier height measurements, the direct energy band alignment between STO and PTO has been determined. A PTO thin film prepared by pulsed laser deposition was used as the substrate and an STO thin film was stepwise deposited onto the substrate by applying the same experimental procedure as explained in Section 2.

By extracting the binding energies of Pb and Sr emission lines from the photoelectron spectra, the evolutions of the binding energies both from the PTO substrate and the STO film can be obtained, as shown in Fig. 13. The inset shows the valence band spectra and the determined valence band maximum energies of the uncovered PTO substrate and the 8-nm thick STO film. The binding energy difference $(E_{B,core} - E_{VBM})$ between the Sr and Pb core levels and the valence band maximum is subtracted in Fig. 13 in order to obtain a better comparison of the energy evolution. After the subtraction, the binding energy evolution nicely represents the

evolution of the valence band maximum during the interface formation.

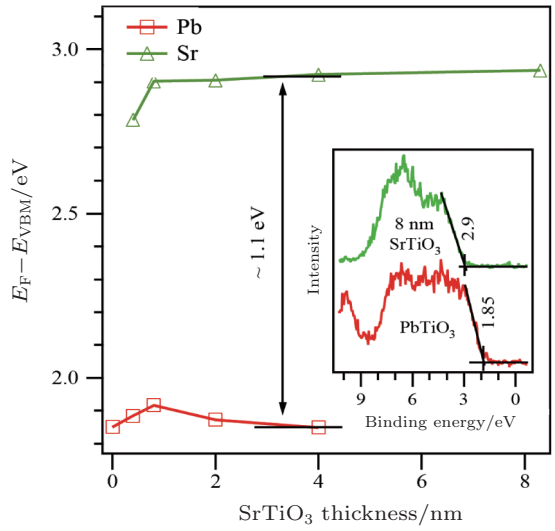


Fig. 13. The binding energy of the Pb $4f_{7/2}$ and Sr $3d_{5/2}$emission lines with respect to the corresponding valence band maximum position, shown in dependence on the STO film thickness. The inset features XP valence band spectra of the uncovered PTO sample and the 8 nm thick STO film.[76]

Both of the binding energy courses show a slight shift at low STO film coverage at the beginning of the interface formation. After the STO reaches a film thickness of 2 nm, the binding energy of Pb 4f exhibits a downward shift toward its original value as the uncovered substrate, while the binding energy of Sr 3d still shows a very small increase. Nevertheless neither of them shows a strong variation at high STO film coverage, indicating that the interface formation can be considered to be complete at 4-nm film thickness. It is therefore feasible to determine the valence band offset at $d_{STO} = 4$ nm, where the energy shift of Sr 3d tends to saturate while the Pb 4f is still quite detectable. At this thickness, the energy difference between Sr 3d and Pb 4f, which corresponds to the offset at the valence band maximum of STO and PTO, amounts to 1.1 ± 0.1 eV, with the valence band maximum of STO lying lower than that of PTO. By considering the band gaps of STO (3.2 eV) and PTO (3.4 eV), the offset at the conduction band minimum of these two materials amounts to 1.3 ± 0.1 eV. This energy band alignment derived from the direct interface analysis is very consistent with the estimated value from the barrier height measurements described above, which confirms the reliability of transitivity for determining the energy band alignment.

The determinations of the energy band alignment between $SrTiO_3$ and $PbTiO_3$ reached by different experimental approaches are in very good agreement. The directly measured valence band discontinuity at the PTO/STO interface amounts to 1.1 ± 0.1 eV, with the energy bands of STO lying lower than those of PTO. This corresponds quite well to the observed 1.1 eV lower Fermi level position at the interfaces of PTO with different contact materials as compared to STO, showing that the band alignments at these interfaces are transitive.

The distinct energy band alignment of STO and PTO can be attributed to their different electronic structures. The valence band of STO is formed almost exclusively by the O 2p states, and the Ti 3d states contribute only to the conduction band. This kind of electronic structure is also observed for many other oxides such as In_2O_3, SnO_2, ZnO, and Al_2O_3, in which the valence band is mostly formed by the anion oxygen. As a result, the valence band discontinuity (ΔE_{VBM}) between STO and these oxides follows the so called common-anion rule and is practically zero. In PTO, however, Pb is present as Pb^{2+}, i.e., in a $5d^{10}6s^26p^0$ configuration with an occupied s orbital at the last valence shell. Payne and Walsh have revealed, using DFT calculations and photoemission, that in Pb-containing oxides, the occupied cation 6s/6p orbitals interact with the O 2p orbitals in a way that a bonding state at the bottom of the valence band and an antibonding state at the top are formed.[77,78] This is often referred to as the lone-pair effect. Due to the relativistic stabilization of the 6s electrons, the Pb 6s states appear predominantly as a separate energy band below the O 2p dominated valence bands, which is represented by the emission at $E_B \approx 10$ eV in the inset of Fig. 13. A similar effect can be observed from Bi-containing oxides, since Bi, the neighbor of Pb in the periodic table, has an electronic configuration similar to that of Pb, and therefore exhibits the lone-pair effect as well.[79,80] As a result, the cation Pb in PTO contributes significantly to the formation of the valence band, leading to a higher valence band maximum energy compared to that of STO.

The energy band alignment shows a strong correlation to the electrical properties of these materials. When the Fermi level, which determines the charge carrier concentrations in the valence band (i.e., hole concentration p) and in the conduction band (i.e., electron concentration n), is located well above E_{VB} or below E_{CB}, the material is an insulator. Varying the Fermi level position by doping is limited by the formation of intrinsic defects.[33,34,81,82] Lowering the Fermi energy by acceptor doping generally reduces the formation enthalpy of intrinsic donor defects like oxygen vacancies or metal interstitials.[34] The doping limit, i.e., the lowest possible Fermi energy, is reached when the formation enthalpy of the donors becomes zero. Raising the Fermi energy by donor doping is correspondingly limited by the intrinsic acceptor formation. Hence the different electrical properties of oxides are related to the energies of the valence and conduction bands on an absolute energy scale. A material having a low valence band energy cannot become a p-type conductor, while a material having a high conduction band energy cannot be an n-type conductor.

While n-type conductivity can be easily achieved in

$SrTiO_3$, e.g., by Nb doping, only weak p-type conductivity is observed for acceptor (e.g., Fe) doped STO at high temperatures and high oxygen pressures. This doping asymmetry with a clear preference for n-type conductivity, i.e., for Fermi level positions closer to the conduction band, is also reflected in the barrier heights determined at the interfaces of $SrTiO_3$ with different contact materials. From systematic investigations at the surface of (Ba,Sr)TiO_3, as shown in Fig. 14 (left), the Fermi level position is reproducibly found in the upper half of the energy gap, closer to the conduction band. In contrast, materials like $PbTiO_3$ or PZT remain highly insulating, regardless of the doping type. The absence of high electrical conductivity is due to a low concentration of charge carriers, i.e., the bulk Fermi level is far away from both the conduction and the valence bands. This is in agreement with the determined barrier heights shown in Fig. 12, where the Fermi level is located more than 1 eV away from both band edges. This is again confirmed by the systematic measurement at Pb(Zr,Ti)O_3 surfaces as shown in Fig. 14 (right). When the energy bands of BST and PZT in Fig. 14 are aligned according to the valence band offset determined from the transitivity rule (Fig. 12) or direct alignment results (Fig. 13), the ranges of $E_F - E_{VB}$ at the surfaces of these two materials are in excellent agreement with each other. The overall variations of the Fermi level positions in BST and PZT are of the same magnitude and lower than 1.5 eV, which is again in good accordance to the allowed variation obtained from defect calculations.

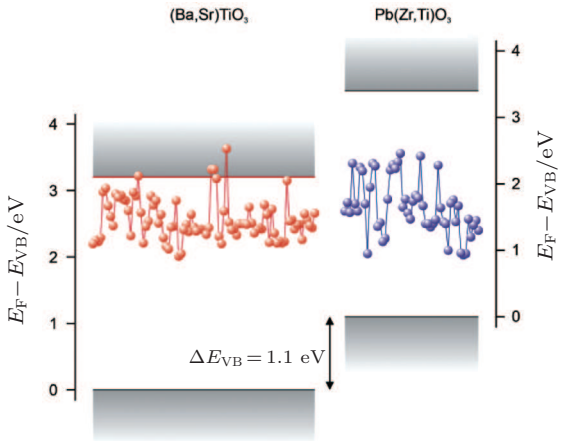


Fig. 14. Fermi level position at the surfaces of (Ba,Sr)TiO_3 and Pb(Zr,Ti)O_3, measured using photoelectron spectroscopy. The energy bands of (Ba,Sr)TiO_3 and Pb(Zr,Ti)O_3 are aligned according to the experimentally determined band offset of ΔE_{VB} = 1.1 eV. The observed variation of Fermi level at the surfaces agrees with the range of Fermi level positions at the interfaces with different materials. It also reflects the achievable doping in the two materials.[76]

As the Fermi level position in the bulk of a material is impossible to access if no electrical transport measurements are possible, as is the case for insulating materials, the close correspondence between bulk, surface, and interface Fermi levels offers a strategy to overcome this limitation indirectly. The knowledge of Fermi level positions is particularly relevant for the defect properties of a material, as the formation energies of charged defects directly depend on the Fermi level position.

4.5. Polarization dependence of Schottky barrier

Ferroelectric materials are characterized by their spontaneous electric polarization. In perovskite materials like $BaTiO_3$ this is caused by ionic displacements. A depolarization electric field is associated with the bound charge that occurs at the surface interface planes where the polarization has a perpendicular component. This field must be screened in order to stabilize the polarization.

For the imperfect screening, which can induce an additional interfacial capacitance, the Schottky barrier height Φ_B at the ferroelectric/electrode interface strongly depends on the magnitude of the polarization.[83–85] The difference in barrier height expected for polarization reversal is given by $\Delta\Phi_B = 2\lambda_{eff} \cdot (D_s/\varepsilon_0)$, where D_s, ε_0, and λ_{eff} are the dielectric displacement in the ferroelectric, the vacuum permittivity, and the effective screening length, respectively. The latter quantity depends on the charge density distribution at the interface, determined by the atomic configuration. For the interfaces of $BaTiO_3$(100) with $SrRuO_3$ (SRO) and Pt, the values predicted by Stengel *et al.* are $\Delta\Phi_B = 1.8$ eV for SRO and 0.03 eV for Pt electrode.[85] In this part, the polarization dependence of the Schottky barrier on the BTO/RuO_2 interface will be introduced, a similar result on BTO/Pt can be found elsewhere.[86]

Experimental evidences for the dependence of the Schottky barrier height on polarization are provided both by leakage current measurements of ferroelectric PZT thin films[87,88] and by electrical currents through ferroelectric tunnel junctions.[89–92] However, the extraction of quantitative values for the Schottky barrier heights and their dependences on polarization requires model assumptions about the charge transport. In addition, the leakage current behavior often depends crucially on both the choice of the electrode material and the details of the electrode preparation.

As introduced in the above sections, XPS measurement is a useful method to evaluate the absolute barrier height at the PZT interface. From a clean substrate, one obtains the binding energy of the VBM E_{VB} with respect to the Fermi level as well as the core level binding energies. The binding energy difference between the VBM and any core level is a material constant, which remains constant upon interface formation.[64,93] Once the binding energy difference between the VBM and a core level is known for a material, it is possible to extract the Fermi level position in the band gaps directly from the core level binding energies. In the present work, XPS is used to determine the absolute values of the Schottky barrier heights at the interface of $BaTiO_3$(100) single crystal with RuO_2 electrode in dependence on the ferroelectric polarization. As an

extension of the previous work, the experimental approach described in this part enables us to obtain the dependence of the barrier height on polarization directly by *in situ* control of the polarization state.

The experimental arrangement depicted in Fig. 15 is used in order to follow the changes in the core level binding energies upon applying electric fields across the sample. In contrast to the typical interface experiment, like the PZT/Pt work discussed in Subsection 4.1, where the thickness of the electrode material is systematically increased to follow the evolution of the chemical and electronic interactions at the interface, the electrode thickness is not varied during the experiment in this arrangement. As outlined above, the barrier height can be determined directly from the core level binding energies once the binding energy difference between the core level and the VBM is known. For the present work, these binding energy differences are taken from a large set of samples independent of the present experiment.

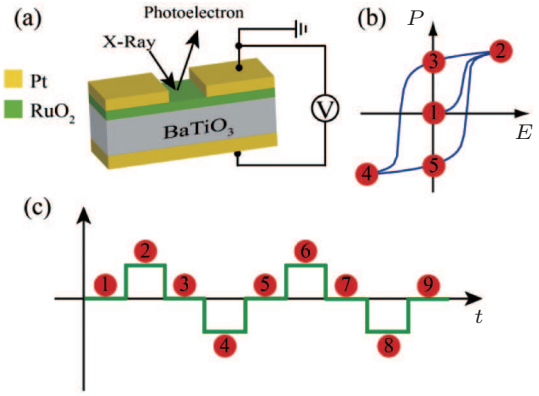


Fig. 15. (a) Arrangement of layers and electric contacts for measurement of polarization dependence of Schottky barrier heights; (b) schematic polarization field loop for ferroelectric samples starting from an unpoled state 1; (c) the function of the voltage applied on the sample for XPS analysis.

To monitor the barrier heights using XPS, the top electrode must be sufficiently thin (≤ 3 nm) to allow a fraction of photoelectrons from the ferroelectric substrate to transverse the electrode film without losing energy. On the other hand, the electrode must be thick enough to provide a continuous layer for the electric contact. In PZT/RuO_2 interface experiments, we have found that a layer thickness of 1.5 nm is sufficient to remove the charging effects observed in the XPS experiment, i.e., it provides a continuous and conducting layer.[94] In the present case, where flat single crystal $BaTiO_3$ samples are used, the conductivity of the RuO_2 layer should also be sufficient to provide the electric contact that is necessary to allow the BTO to switch polarization when sufficiently large voltages are applied. In order to ensure conductivity over the whole contact area, we applied a secondary 50-nm-thick layer of Pt. A circular hole with diameter of 1 mm in the center of the secondary layer was prepared using a lithographically structured photoresist. The photoresist was finally removed with acetone to expose the thin RuO_2 electrode in the center. Due to the low carrier mobility of the undoped BTO,[95] leakage currents through the 0.4-nm-thick sample would be bulk-dominated and too small to be measured. A correlation of the barrier height with the electrical measurements was therefore not possible. Before the electrode deposition, the crystals were heated to 400 °C in the deposition chamber in 2 Pa oxygen atmosphere for 1 h to remove adsorbates like hydrocarbons and water, resulting in a contamination-free surface.[43,94] One side of the crystal was then coated with 50 nm Pt, and the other side was coated with a ~3-nm-thick RuO_2, resulting in a sample with the Pt/BTO/RuO_2 structure. The sample was mounted on a sample holder consisting of two electrically isolated sections, which were wired to the plane bottom and the structured top electrode, respectively. In the spectrometer system (Physical Electronics PHI5700), the two parts of the sample holder were separately wired to the manipulator. During XPS measurement, the top electrode was connected to ground, which provided the Fermi-level binding energy reference of the spectrometer. Due to the application of the voltage to the bottom electrode, no binding energy shifts of the top electrode were expected with the applied voltage. A positive voltage applied to the bottom electrode then corresponded to a polarization of the BTO pointing toward the top contact, which was the one where changes of the barrier height were monitored by XPS. The sequence of voltage applied during the measurement is shown in Fig. 15.

The voltage at the bottom electrode was sequentially set to constant values of +200 V, 0 V, −200 V, and 0 V. For each voltage step, a set of Ba 3d, Ti 2p, and Ru 3d core levels was recorded. The complete voltage cycle was repeated in order to verify the reproducibility of the observed shifts. The spectra recorded for the Pt/BTO/RuO_2 sample are shown in Fig. 16.

Independent of the applied voltage, the core level of the top electrode material exhibits a constant shape and a binding energy of 281.05 eV for Ru $3d_{5/2}$, which is a characteristic value for metallic RuO_2.[74] As the binding energies in XPS are measured with respect to the Fermi level of the spectrometer system, this confirms that the complete top electrode layers are electrically connected to ground during the whole measurement cycle. Above the RuO_2 layer, the secondary thick Pt electrode also exhibits a binding energy of 71.05 eV. Consequently, the Fermi level of the spectrometer is verified to provide the binding energy reference in our experiment, which is required for interpreting the binding-energy shifts of the BTO-related emissions in terms of changes in the Schottky barrier height.

The Ba 3d and Ti 2p core levels of the as-prepared Pt/BTO/RuO_2 sample exhibit binding energies of 778.9 ± 0.1 eV and 458.35 ± 0.1 eV, respectively. In BTO, the bind-

ing energy differences between the VBM and the Ba 3d and Ti 2p core levels amount to 776.45 ± 0.1 eV and 455.9 ± 0.1 eV, respectively. These values are derived from a large set of different $BaTiO_3$ and (Ba,Sr)TiO_3 thin films deposited onto conducting substrates. The Ba 3d and Ti 2p binding energies of the as-prepared sample hence correspond to a Fermi level at the BTO/RuO_2 interface of $E_F - E_{VB} = 2.45 \pm 0.15$ eV above the valence band maximum E_{VB}. This is very close to the value of $E_F - E_{VB} = 2.35$ eV reported for the (Ba,Sr)TiO_3/RuO_2 interface,[74] and it indicates a good reproducibility of the measurements.

In contrast to the core level of the top metallic RuO_2 or Pt electrode, the Ba 3d and Ti 2p core levels show a pronounced reversible shift with the applied voltage. As the binding energy shifts of the Ba 3d and Ti 2p core levels are of the same magnitude, as shown in Fig. 16, it is straightforward to attribute the shifts to the changes of the Fermi level with respect to the band edges, which correspond to the changes of the Schottky barrier heights at the interface. In any of the recorded states of the Pt/BTO/RuO_2 interface, the shape and the width of the BTO core levels remain unchanged. This indicates a laterally homogenous Fermi level position, i.e., a homogenous barrier height.[94] Due to the obvious dependence of the barrier height on polarization, this provides an evidence that the polarization of BTO at the BTO/RuO_2 interface is mostly homogenous during all experimental steps.

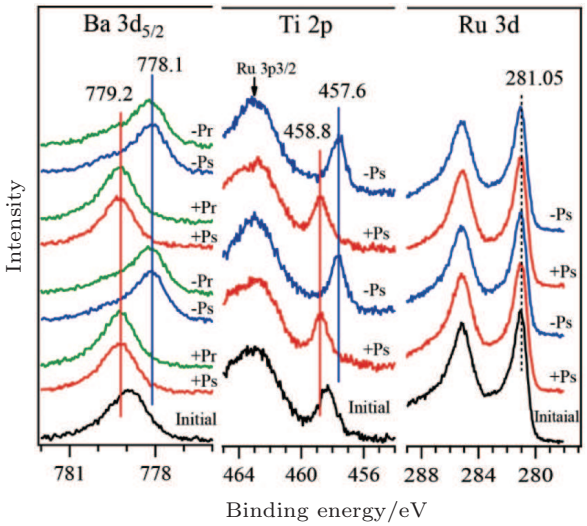


Fig. 16. Core-level spectra of $BaTiO_3$ single crystals with RuO_2 top electrode independent of the applied voltage. The voltages applied across the samples are 0 V for initial and remanent states (±Pr), 200 V for positive saturation (+Ps), and −200 V for negative saturation (–Pr), respectively. In all cases, the top electrode is electrically connected to the spectrometer system and the voltage is applied to the bottom electrode.[86]

In order to quantify the changes of the Schottky barrier height with polarization, the binding energies of the Ba 3d and Ti 2p core levels are plotted for different voltage steps in Fig. 17(a). By subtracting the binding energy differences between the core levels and the VBM given above, the plot directly reveals the Fermi level position at the interface with respect to the VBM of BTO. These values are equivalent to the Schottky barrier height for holes. The Schottky barrier height for electrons is obtained by subtracting the hole barrier from the band gap. As shown in Fig. 17(a), both Ba 3d and Ti 2p core levels reveal the same dependence of barrier height upon polarization. A polarization pointing toward (away from) the top electrode interface, corresponding to a positive (negative) voltage at the bottom electrode as in steps 2 and 6 (steps 4 and 8), leads to an upward (downward) shift of the Fermi level at the top electrode. It should be mentioned that the direction of the shift agrees with the theoretically expected change of the barrier height with polarization. For the BTO/RuO_2 interface, the Fermi level positions at the interface for polarization pointing toward and away from the interface are derived as $E_F - E_{VB} = 2.85 \pm 0.15$ eV and 1.75 ± 0.15 eV, respectively. The difference in barrier height with polarization reversal of $\Delta\Phi_B = 1.1$ eV for the RuO_2 electrode is smaller than the change of 1.8 eV predicted by the DFT for the BTO/$SrRuO_3$ interface,[85] but it is of similar magnitude. A quantitative agreement between theory and experiment is not expected, as the screening length for the BTO/$SrRuO_3$ interface will be different from the BTO/RuO_2 interface due to the epitaxial nature of the former and the different crystal and electronic structures of $SrRuO_3$ and RuO_2.

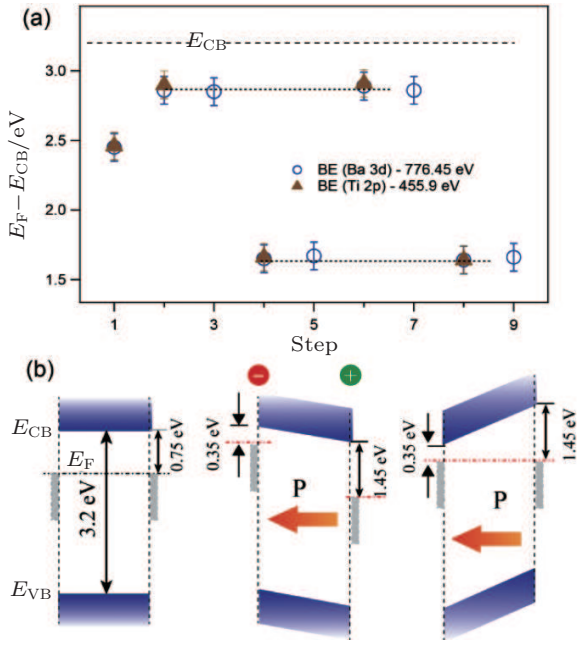


Fig. 17. (a) Valence band maximum energy with respect to the Fermi level as obtained from Ba 3d and Ti 2p core level binding energies recorded during voltage switching with RuO_2 electrode. (b) Schematic energy diagrams with two RuO_2 electrodes before (left), during (middle), and after poling (right). The arrows indicate the direction of polarization.[86]

Additional experiments using the arrangement sketched in Fig. 15 have been performed with an $SrTiO_3$ single crys-

talline and polycrystalline PZT and PLZT ceramics. No significant changes of the core level binding energies are observed for the $SrTiO_3$ single-crystal sample with the applied voltage. The P(L)ZT ceramics have been polished to thickness < 300 μm, such that the maximum voltage of ± 300 V is sufficient to pole the samples. The experiments with P(L)ZT show a behavioral dependence on the applied voltage largely identical to the one reported here. The binding energy changes are also of similar magnitude. Note that the polarization is naturally inhomogeneous at the interface for the polycrystalline P(L)ZT samples. Consequently, significant changes in core level line shape are observed with the poled samples. However, the unpoled samples also exhibit sharp emission lines, indicating an absence of polarization components perpendicular to the interface. These experiments confirm the interpretation of the above-described binding energy shifts in terms of a polarization dependence of barrier height.

5. Summary

We have presented a photoemission study of the interface between $Pb(Zr,Ti)O_3$ and different metallic or conductive oxide electrodes. The deposition of metallic Pt, Ag, and Cu leads to a reduction of the PZT substrate, in particular the formation of metallic lead species. After the metallic deposition, the Fermi level position at the interface is found to be pinned at ~ 1.6 eV above the valence band maximum, which means a midgap Fermi level position and nearly identical Schottky barrier heights for electrons and holes. The PZT/Pt interface can be reversibly oxidized and reduced, accompanied by changes in the interfacial Fermi level position of more than 1 eV. The observed Fermi level pinning at the PZT/metal interfaces is attributed to oxygen vacancies at the interface, which are induced by the chemical reaction. In contrast, the PZT/RuO_2 and PZT/ITO interfaces are not reactive. A transition from a preference for hole injection to a preference for electron injection can be realized by switching from RuO_2 (high work function ~ 6.1 eV) to ITO (low work function ~ 4.5 eV).

A valence band offset of 1.1 ± 0.1 eV and a conduction band offset of 1.3 ± 0.1 eV are determined for the PTO/STO interface. The energy band alignment is in good agreement with the difference in ionization potential, which is determined to be 6.2 eV for PTO and 7.5 eV for STO. This band alignment is further in agreement with the differing barrier heights at interfaces of PZT and BST with different contact materials, which indicates that the transitivity of band lineups is fulfilled for this system. The staggered energy band alignment is described by a common-anion-like alignment of the O 2p derived valence bands of both materials. The range of Fermi level positions at different interfaces of STO(BST) and PTO(PZT) is consistent with the range of observed Fermi level positions at the surfaces of these materials and with the range of Fermi level positions in the bulk, which underlines that the variations of Fermi level positions are comparable in the bulk, at the surface, and at the interfaces. The observed range of Fermi level positions, which is determined by the intrinsic defect properties, illustrates nicely that STO can be highly doped while PTO remains an insulator even at a high doping level.

Direct quantitative measurements of the Schottky barrier height dependence on ferroelectric polarization are obtained with XPS, giving that the polarization dependence of Schottky barrier heights usually explained in terms of the current-voltage characteristics. The experimental procedure is exemplified by BTO single crystal with metallic RuO_2 electrode, for which $\Delta\Phi_B = 1.1$ eV is observed with polarization switching. The outlined measurement procedure demonstrates how photoelectron spectroscopy can be used to obtain so-far inaccessible information about the properties of ferroelectric interfaces.

References

[1] Scott J F 2007 *Science* **315** 954
[2] Scott J F and Dearaujo C A P 1989 *Science* **246** 1400
[3] Lupascu D C and Rodel J 2005 *Adv. Eng. Mater.* **7** 882
[4] Tagantsev A K, Stolichnov I, Colla E L and Setter N 2001 *J. Appl. Phys.* **90** 1387
[5] Chen F, Liu Q Z, Wang H F, Zhang F H and Wu W B 2007 *Appl. Phys. Lett.* **90** 192907
[6] Schorn P J, Brauhaus D, Bottger U, Waser R, Beitel G, Nagel N and Bruchhaus R 2006 *J. Appl. Phys.* **99** 114104
[7] Ramesh R, Gilchrist H, Sands T, Keramidas V G, Haakenaasen R and Fork D K 1993 *Appl. Phys. Lett.* **63** 3592
[8] Eom C B, Vandover R B, Phillips J M, Werder D J, Marshall J H, Chen C H, Cava R J, Fleming R M and Fork D K 1993 *Appl. Phys. Lett.* **63** 2570
[9] Chen M S, Wu T B and Wu J M 1996 *Appl. Phys. Lett.* **68** 1430
[10] Wu W B, Wong K H, Choy C L and Zhang Y H 2000 *Appl. Phys. Lett.* **77** 3441
[11] Alshareef H N, Auciello O and Kingon A I 1995 *J. Appl. Phys.* **77** 2146
[12] Lou X J 2009 *J. Appl. Phys.* **105** 024101
[13] Klein A 2012 *Thin Solid Films* **520** 3721
[14] Sze S M and Ng K K 2007 *Physics of Semiconductor Devices* (3rd edn.) (Hoboken: Wiley-Interscience)
[15] Scott J F, Watanabe K, Hartmann A J and Lamb R N 1999 *Ferroelectrics* **225** 83
[16] Mönch W 2004 *Electronic Properties of Semiconductor Interfaces* (New York: Springer)
[17] Cillessen J F M, Prins M W J and Wolf R M 1997 *J. Appl. Phys.* **81** 2777
[18] Lee J J, Thio C L and Desu S B 1995 *J. Appl. Phys.* **78** 5073
[19] Foster C M, Csencsits R, Bai G R, Li Z, Wills L A, Hiskes R, AlShareef H N and Dimos D 1995 *Integr Ferroelectr.* **10** 31
[20] Rao A V, Mansour S A and Bement A L 1996 *Mater. Lett.* **29** 255
[21] Chen F, Wang H F, Liu Q Z, Wu W B and Li X G 2007 *Appl. Phys. Lett.* **90** 082904
[22] Pintilie L, Vrejoiu I, Hesse D and Alexe M 2006 *Appl. Phys. Lett.* **88** 102908
[23] Du X F and Chen I W 1998 *J. Appl. Phys.* **83** 7789
[24] Cardona M 1965 *Phys. Rev.* **140** A651
[25] Scott J F 1989 *Ferroelectric Memories* (New York: Springer)
[26] Robertson J 2000 *J. Vac. Sci. Technol. B* **18** 1785
[27] Piskunov S, Heifets E, Eglitis R I and Borstel G 2004 *Comp. Mater. Sci.* **29** 165
[28] Tufte O N and Chapman P W 1967 *Phys. Rev.* **155** 796
[29] Gerson R and Jaffe H 1963 *J. Phys. Chem. Solids* **24** 979
[30] Wu L, Wu T S, Wei C C and Liu H C 1983 *J. Phys. C: Solid State phys.* **16** 2823

[31] Walukiewicz W 2001 *Phys. B* **302–303** 123
[32] Zhang S B, Wei S H and Zunger A 1998 *J. Appl. Phys.* **83** 3192
[33] Zunger A 2003 *Appl. Phys. Lett.* **83** 57
[34] Robertson J and Clark S J 2011 *Phys. Rev. B* **83** 075205
[35] Waldrop J R, Grant R W, Kowalczyk S P and Kraut E A 1985 *J. Vac. Sci. Technol. A* **3** 835
[36] Yu E T, Mccaldin J O and Mcgill T C 1992 *Solid State Physics* **46** 1
[37] Franciosi A and VandeWalle C G 1996 *Surf. Sci. Rep.* **25** 1
[38] Tanuma S, Powell C J and Penn D R 1991 *Surf. Interface. Anal.* **17** 911
[39] Rao G V, Sauberlich F and Klein A 2005 *Appl. Phys. Lett.* **87** 032101
[40] Li S Y, Wachau A, Schafranek R, Klein A, Zheng Y L and Jakoby R 2010 *J. Appl. Phys.* **108** 014113
[41] Klein A, Loher T, Tomm Y, Pettenkofer C and Jaegermann W 1997 *Appl. Phys. Lett.* **70** 1299
[42] Schafranek R, Payan S, Maglione M and Klein A 2008 *Phys. Rev. B* **77** 195310
[43] Gassenbauer Y, Schafranek R, Klein A, Zafeiratos S, Hävecker M, Knop-Gericke A and Schlógl R 2006 *Phys. Rev. B* **73** 245312
[44] Moulder J F and Chastain J 1995 *Handbook of X Ray Photoelectron Spectroscopy: A Reference Book of Standard Spectra for Identification and Interpretation of XPS Data* (Physical Electronics Division, Perkin-Elmer Corporation)
[45] Korber C, Harvey S P, Mason T O and Klein A 2008 *Surf. Sci.* **602** 3246
[46] Takatani S, KushidaAbdelghafar K and Miki H 1997 *Jpn. J. Appl. Phys.* **36** L435
[47] Takatani S, Miki H, Kushida-Abdelghafar K and Torii K 1999 *J. Appl. Phys.* **85** 7784
[48] Miyano K E, King D M, Spindt C J, Kendelewicz T, Cao R, Yu Z P, Lindau I and Spicer W E 1991 *Phys. Rev. B* **43** 11806
[49] Schlaf R, Klein A, Pettenkofer C and Jaegermann W 1993 *Phys. Rev. B* **48** 14242
[50] Klein A, Pettenkofer C, Jaegermann W, Luxsteiner M and Bucher E 1994 *Surf. Sci.* **321** 19
[51] Mcgilp J F 1984 *J. Phys. C: Solid State Phys.* **17** 2249
[52] Chasse T, Theis W, Chen T P, Evans D A, Horn K, Pettenkofer C and Jaegermann W 1991 *Surf. Sci.* **251** 472
[53] Klein A, Pettenkofer C, Jaegermann W, Chasse T, Horn K, Luxsteiner M C and Bucher E 1992 *Surf. Sci.* **264** L193
[54] Meyer K, Schuller I K and Falco C M 1981 *J. Appl. Phys.* **52** 5803
[55] Brillson L J, Mosbacker H L, Hetzer M J, Strzhemechny Y, Jessen G H, Look D C, Cantwell G, Zhang J and Song J J 2007 *Appl. Phys. Lett.* **90** 102116
[56] Chen F, Schafranek R, Wu W B and Klein A 2011 *J. Phys. D: Appl. Phys.* **44** 255301
[57] Spicer W E, Chye P W, Skeath P R, Su C Y and Lindau I 1979 *J. Vac. Sci. Technol.* **16** 1422
[58] Rao F Y, Kim M Y, Freeman A J, Tang S P and Anthony M 1997 *Phys. Rev. B* **55** 13953
[59] Schafranek R and Klein A 2006 *Solid State Ion.* **177** 1659
[60] Niessen A K, Deboer F R, Boom R, Dechatel P F and Mattens W C M 1983 *Calphad* **7** 51
[61] Cheng J R and Meng Z Y 2000 *J. Mater. Sci. Lett.* **19** 1945
[62] Kaewchinda D, Chairaungsri T, Naksata M, Milne S J and Brydson R 2000 *J. Eur. Ceram. Soc.* **20** 1277
[63] Kraut E A, Grant R W, Waldrop J R and Kowalczyk S P 1980 *Phys. Rev. Lett.* **44** 1620
[64] Chambers S A, Droubay T, Kaspar T C, Gutowski M and van Schilfgaarde M 2004 *Surf. Sci.* **554** 81
[65] Kurtin S, McGill T C and Mead C A 1969 *Phys. Rev. Lett.* **22** 1433
[66] Louie S G, Chelikowsky J R and Cohen M L 1977 *Phys. Rev. B* **15** 2154
[67] Tejedor C, Flores F and Louis E 1977 *J. Phys. C: Solid State Phys.* **10** 2163
[68] Tersoff J 1984 *Phys. Rev. Lett.* **52** 465
[69] Cardona M and Christensen N E 1987 *Phys. Rev. B* **35** 6182
[70] Robertson J and Chen C W 1999 *Appl. Phys. Lett.* **74** 1168
[71] Chen F, Schafranek R, Wu W B and Klein A 2009 *J. Phys. D: Appl. Phys.* **42** 215302
[72] Mónch W 1987 *Phys. Rev. Lett.* **58** 1260
[73] Chen F, Schafranek R, Li S, Wu W B and Klein A 2010 *J. Phys. D: Appl. Phys.* **43** 295301
[74] Schafranek R, Schaffner J and Klein A 2010 *J. Eur. Ceram. Soc.* **30** 187
[75] Katnani A D and Margaritondo G 1983 *Phys. Rev. B* **28** 1944
[76] Schafranek R, Li S Y, Chen F, Wu W B and Klein A 2011 *Phys. Rev. B* **84** 045317
[77] Payne D J, Egdell R G, Law D S L, Glans P A, Learmonth T, Smith K E, Guo J, Walsh A and Watson G W 2007 *J. Mater. Chem.* **17** 267
[78] Walsh A and Watson G W 2005 *J. Solid State Chem.* **178** 1422
[79] Walsh A, Payne D J, Egdell R G and Watson G W 2011 *Chem. Soc. Rev.* **40** 4455
[80] Li S, Morasch J, Klein A, Chirila C, Pintilie L, Jia L, Ellmer K, Naderer M, Reichmann K, Gróting M and Albe K 2013 *Phys. Rev. B* **88** 045428
[81] Ágoston P, Körtber C, Klein A, Puska M J, Nieminen R M and Albe K 2010 *J. Appl. Phys.* **108** 053511
[82] Robertson J 2008 *Thin Solid Films* **516** 1419
[83] Stengel M and Spaldin N A 2006 *Nature* **443** 679
[84] Stengel M, Vanderbilt D and Spaldin N A 2009 *Nat. Mater.* **8** 392
[85] Stengel M, Aguado-Puente P, Spaldin N A and Junquera J 2011 *Phys. Rev. B* **83** 235112
[86] Chen F and Klein A 2012 *Phys. Rev. B* **86** 094105
[87] Pintilie L, Vrejoiu I, Hesse D, LeRhun G and Alexe M 2007 *Phys. Rev. B* **75** 104103
[88] Lee D, Baek S H, Kim T H, Yoon J G, Folkman C M, Eom C B and Noh T W 2011 *Phys. Rev. B* **84** 125305
[89] Garcia V, Fusil S, Bouzehouane K, Enouz-Vedrenne S, Mathur N D, Barthelemy A and Bibes M 2009 *Nature* **460** 81
[90] Gruverman A, Wu D, Lu H, Wang Y, Jang H W, Folkman C M, Zhuravlev M Y, Felker D, Rzchowski M, Eom C B and Tsymbal E Y 2009 *Nano Lett.* **9** 3539
[91] Maksymovych P, Jesse S, Yu P, Ramesh R, Baddorf A P and Kalinin S V 2009 *Science* **324** 1421
[92] Crassous A, Garcia V, Bouzehouane K, Fusil S, Vlooswijk A H G, Rispens G, Noheda B, Bibes M and Barthélémy A 2010 *Appl. Phys. Lett.* **96** 042901
[93] Kraut E A, Grant R W, Waldrop J R and Kowalczyk S P 1983 *Phys. Rev. B* **28** 1965
[94] Chen F, Schafranek R, Wachau A, Zhukov S, Glaum J, Granzow T, von Seggern H and Klein A 2010 *J. Appl. Phys.* **108** 104106
[95] Morrison F D, Zubko P, Jung D J, Scott J F, Baxter P, Saad M M, Bowman R M and Gregg J M 2005 *Appl. Phys. Lett.* **86** 152903